ELSEVIER

Biophysical Chemistry 85 (2000) 209–228

Biophysical Chemistry

www.elsevier.nl/locate/bpc

A Pro → Ala substitution in melittin affects self-association, membrane binding and pore-formation kinetics due to changes in structural and electrostatic properties ☆

Sybille Rex*

Department of Biophysical Chemistry, Biocenter of the University of Basel, Basel, Switzerland

Abstract

Melittin, the main component of bee venom of *Apis mellifera*, contains a proline at position 14, which is highly conserved in related peptides of various bee venoms. To investigate the structural and functional role of Pro14 a melittin analogue was studied where proline is substituted by an alanine residue (P14A). The investigations were focussed on: (i) the secondary structure in aqueous solution and membranes; (ii) the self-association in solution; (iii) the binding to POPC membranes; and (iv) the P14A-induced leakage and pore formation in membrane vesicles. Circular dichroism and gel filtration experiments showed that P14A exists at concentrations < 12 μM in monomeric form with an α-helicity of $28 \pm 7\%$. A further increase in peptide concentration leads to the formation of large aggregates consisting of 9 ± 1 monomers. While binding studies with POPC vesicles revealed for P14A a stronger binding affinity towards membranes than for melittin, the peptide-induced leakage of fluorescent markers from vesicles was less efficient for P14A than for melittin. Furthermore, an unexpected efflux behaviour at high values of bound P14A was observed which indicated that the pore formation kinetics for P14A is more complex than it was reported for melittin. The different features of P14A in aggregation, binding and efflux compared to melittin are mainly ascribable directly to structural changes caused by the proline → alanine substitution. Furthermore, the results indicate an improved screening of the positively charged residues of P14A by counterions which contributes additionally to the observed differences in peptide activities. It is suggested that the presence of proline in melittin is not only of structural importance but also influences indirectly the electrostatic properties of the native peptide.

Keywords: [Ala-14]melittin; Proline14; Aggregation; Binding isotherm; Peptide-induced leakage; Charge screening

☆ This paper is dedicated to Professor Gerhard Schwarz on the occasion of his 70th birthday.

* Department of Molecular and Cell Biology, Boston University, 700 Albany Street, Boston, MA 02118-2392, USA. Tel.: +1-617-638-4723; fax: +1-617-414-1041.

E-mail address: srex@bu.edu (S. Rex).

0301-4622/00/$ - see front matter
PII: S0301-4622(00)00121-6

1. Introduction

Proline has a unique position among the amino acids because of its inability to form backbone hydrogen bonds. In soluble proteins it is thought to be the least likely residue to occur in an α-helix [1]. Despite its hydrophobic side chain its typical location is that of a hydrophilic residue and is almost always exposed on the protein surface [2], hence it would not be expected within a membrane. Nevertheless, proline residues have been found in numerous transmembrane helices of membrane proteins. Their possible structural and dynamical role has been discussed in great detail by Williams and Deber [3]. Proline is known to introduce a kink into an α-helix causing an increased flexibility in the helical structure due to the lack of intramolecular hydrogen bonds. The resulting bending angle has been estimated to be constant at approximately 20–30° and is, therefore, thought to be of structural or functional importance [4]. In numerous studies the contributions of proline to the stabilisation of channel structures and the optimisation of properties of transport proteins have been investigated [3,5–7]. Proline residues do not only occur within membrane spanning α-helices of transport proteins and receptors, but also in amphipathic helices of channel-forming peptides like alamethicin, melittin and pardaxin 1 [8].

Melittin (isolated from bee venom of *Apis mellifera*) is a well-studied peptide of 26 amino acids with a proline residue at position 14 (for reviews see [8–12]). Under conditions favouring the α-helical conformation of melittin (e.g. in membrane-bound state or self-associated in form of tetramers in aqueous solution) the proline induces a kink in the helical structure [13]. As shown in Table 1, proline at position 14 is highly conserved among the melittin components of venoms from various honeybee species. Several studies have been attributed to the investigation of proline's contribution to structural and functional properties of melittin [14–17] by using a synthetic melittin analogue where Pro14 is substituted by an alanine ([Ala-14]melittin or P14A).

Similar to melittin, its analogue P14A has an amphiphatic character and is well soluble in water. Structural studies with P14A in methanol by ^{1}H-NMR and amide exchange measurements [14] revealed the existence of a more stable helix for P14A than for melittin which is especially pronounced in the central region of the peptide. In melittin the N- and C-terminal helical segments are connected by a flexible hinge due to the existence of proline whereas P14A shows a large suppression of backbone fluctuations in this region. Further structural studies in methanol [16] indicated a cooperative effect of the proline to alanine substitution on helix stability. The replacement leads not only to a stabilisation of the

Table 1
Melittin from venoms of various honeybee species[a]

Melittin from...	Sequence
Apis mellifera (honeybee)	1 10 20 26
Apis mellifera cerana	G I G A V L K V L T T G L **P** A L I S W I K R K R Q Q NH_2
(Indian honeybee)	(+) + + + + +
Apis mellifera dorsata	G I G A I L K V L S T G L **P** A L I S W I K R K R Q E NH_2
(Giant honeybee)	(+) + + + + +
Apis mellifera florea	G I G A I L K V L A T G L **P** T L I S W I K N K R K Q NH_2
(Little honeybee)	(+) + + + + +

[a]The peptides differ only slightly in their amino acid sequence. Underlined residues are 100% conserved. Variations occur mainly in the C-terminal region but net charges (+5 to +6) and charge distributions are very similar for the melittin peptides.

kinked region but was observed throughout the entire helix, though to a less extent.

The interaction of P14A with biological as well as model membranes has been investigated in several studies [14,15,17]. P14A was reported to cause reversible disc micellization of dimyristoylphosphatidylcholine bilayers when the temperature was decreased or increased relative to the phase transition temperature of the membrane. The rate of this process was found to be much slower for P14A than for melittin and is ascribed to the structural differences of both peptides. Performing conductivity measurements on planar lipid bilayers Dempsey et al. [14] showed that melittin is more active than P14A, thus indicating a higher barrier of membrane insertion for the melittin analogue and the formation of more stable channels by melittin. However, in experiments with erythrocytes P14A caused similar biphasic release kinetics as melittin but appeared to be more efficient [14]. According to Rudenko and Nipot [17], the higher lytic activity of P14A in erythrocytes can be ascribed to a higher binding affinity towards the cells. In addition, peptide–protein interactions seem to play an important role in the haemolytic mechanism, which is proposed to be different for both peptides.

In this report, the investigations of structural and functional contributions of proline to the properties of melittin were extended. Besides structural studies, the investigations were aimed at the interaction of P14A with model membranes. In a first set of experiments the secondary structure of P14A in various aqueous solutions was explored by circular dichroism. In combination with gel filtration experiments insights into the concentration-dependent self-association process of P14A and the size of the formed aggregates were obtained. The second part of my study was focussed on peptide–membrane interactions. Here, especially the binding to POPC membranes and the P14A-induced leakage of dye molecules from differently sized vesicles were investigated in greater detail. The leakage experiments gave information about the mechanism of pore formation, which was found to be more complex for P14A than for melittin. The study presented here demonstrates that melittin's proline, first, plays a structural role and second, influences indirectly the electrostatic properties of the native peptide. As a consequence, proline optimises melittin's functional properties by regulating the aggregate size in solution and the binding affinity towards membranes, and by controlling the pore size and/or pore lifetime which leads to a more efficient lytic activity in model membranes.

2. Materials and methods

2.1. Materials

5(6)-Carboxyfluorescein (mol wt. = 376), FITC-dextran (mol wt. = 9400, commercial name FD10, 0.008 mol FITC/mol glucose), TES and molecular weight marker proteins for calibration of the gel filtration column were purchased from Sigma (St. Louis, MO, USA). NaCl, $Na_2EDTA \cdot 2H_2O$ and Triton X-100 were supplied by Merck (Darmstadt, Germany) and HEPES by Bioprobe (Basel, Switzerland). POPC and NBD-DOPE were obtained from Avanti Polar Lipids, Inc. (Birmingham, AL, USA). Sephadex G50, Sephacryl S-300 HR and Blue dextran 2000 were received from Pharmacia (Uppsala, Sweden).

The synthetic peptide P14A (mol wt. = 2814 Da) was a generous gift of Dr Chris Dempsey (Biochemistry Department and Centre of Molecular Recognition, Bristol University, UK). Synthetic melittin (mol wt. = 2840 Da) was purchased from Bachem Feinchemikalien (Bubendorf, Switzerland) and used without further purification. The concentration of both peptides in aqueous solution was determined by UV spectroscopy using an absorption coefficient of 5570 M^{-1} cm^{-1} at 280 nm [15,18].

If not otherwise noted, the buffer was composed of 10 mM HEPES, 107 mM NaCl, 1 mM $Na_2EDTA \cdot 2H_2O$ (pH 7.4, 20°C). An aqueous stock solution of the fluorescent dye 5(6)-carboxyfluorescein contained 50 mM CF, 10 mM HEPES, 10 mM NaCl, 1 mM $Na_2EDTA \cdot 2H_2O$ (pH 7.4, 20°C). The composition of the dye solution was adjusted to be iso-osmolar with the buffer. The concentration of CF was determined by UV spectroscopy using an absorption coefficient

of 72 000 M^{-1} cm^{-1} at 492 nm [19]. An aqueous solution of FITC-dextran was composed of 7.4 mM dye, 7.4 mM HEPES, 37 mM NaCl, 0.75 mM $Na_2EDTA \cdot 2H_2O$ (pH 7.4 at 20°C). The size of FITC-dextran was determined as 2–3 nm in radius [20–22].

As described previously in detail [22,23] LUV with diameters of approximately 100 and 200 nm, respectively, were prepared by means of the extrusion technique [24,25]. Briefly, POPC in chloroform was dried down to form a thin lipid film, which was resuspended in buffer or a dye solution. After five freeze–thaw cycles the suspension was extruded through a polycarbonate filter of 100- or 200-nm pore diameter, respectively. The external dye was separated from the vesicles by gel filtration over either a Sephadex G50 column (in the case of CF) or a Sephacryl S-300 HR column (in the case of FD10) (both 1×30-cm columns). The total lipid concentration was determined by phosphate analysis [26]. As reported earlier [22] the vesicle diameter was determined as 106 ± 6 nm for LUV_{100} and as 240 ± 20 nm for LUV_{200}.

2.2. Circular dichroism spectroscopy

CD spectra of P14A were recorded at a Jasco J-710 Spectropolarimeter (Jasco, Japan Spectroscopic Co., Tokyo) scanning the wavelength from 250 to 200 nm at 20°C under N_2 flow. Quartz cuvettes with a thickness of 1 or 0.2 mm, respectively, were used. A total of 30 accumulations were recorded using a scan speed of 50 nm/data, 0.5 or 0.1 nm/datapoint and 1 or 0.5 s response time. Each spectrum has been corrected for solvent contributions. The so corrected ellipticity $[\Theta]_{corr}$ (in mdeg) was converted into the mean residue ellipticity $[\Theta] = [\Theta]_{corr}/c_p \cdot d \cdot N$ (in deg cm^2 $dmol^{-1}$) with c_p as the peptide concentration, d as the thickness of the cuvette and N as the number of amino acid residues per peptide. The α-helical fraction f_H of a peptide was estimated from the mean residue ellipticity at 222 nm, $[\Theta]_{222}$, according to a relationship proposed by Chen et al. [27]:

$$f_H = \{[\Theta]_{222} - (-2340)\}/(-30\,300) \quad (1)$$

where the ellipticity values are given in deg · cm^2 $dmol^{-1}$.

To determine the peptide structure in a membrane 10 μM P14A was incubated for 10 min with 200 μM POPC LUV_{100} vesicles in buffer at room temperature. The spectra were corrected for contributions from vesicles and free peptide, and the helicity was calculated as described above.

2.3. Gel filtration experiments

Gel filtration runs of various concentrations of P14A were performed using a 0.7×50-cm Sephadex G50 column eluted by a buffer composed of 10 mM TES, 107 mM NaCl and 1 mM EDTA (pH 7.4) at a rate of 14 ml h^{-1}. The column was calibrated by molecular weight using the proteins carbonic anhydrase, soybean trypsin inhibitor, cytochrome *c* and aprotinin. In addition, melittin (70 μM) in salt-free buffer (10 mM TES, 1 mM EDTA, pH 7.4) was utilised as marker peptide for P14A monomers. Furthermore, Dextran blue 2000 has been used as an indicator of the void volume in each column run. A sample volume of 200 μl was applied to the column and approximately 160 μl were collected per fraction. The peptide content per fraction has been determined by a modified Lowry assay as described by Markwell et al. [28].

2.4. Dynamic light scattering

To determine the hydrodynamic radii of aggregates of P14A and vesicles a commercial apparatus [ALV-125 laser light scattering goniometer equipped with a He–Ne-Laser ($\lambda = 632$ nm) and an ALV-5000 correlator] was used. All measurements were performed at 20°C under a scattering angle of 90° using cylindrical quartz cuvettes (1 cm diameter) which were especially made for light scattering measurements. The experimental autocorrelation function was fitted by a CONTIN-analysis (built-in-software in ALV-5000).

2.5. Binding measurements

Binding of P14A to large unilamellar vesicles of POPC was measured by a resonance energy transfer assay as described previously [23,29]. Briefly, vesicles containing 0.3 mol% NBD-DOPE were prepared as described above. The energy transfer between the tryptophan residue of P14A (donor) and the NBD group of the lipids (acceptor) resulted in an enhanced NBD emission after binding of the peptide to the membrane. A Jasco FP 777 spectrofluorometer (Jasco, Japan Spectroscopic Co., Tokyo) has been used with excitation at 280 nm (slit 1.5 nm), emission at 530 nm (slit 3 nm), and a 295-nm cut-off filter. To obtain a binding isotherm a vesicle solution was titrated to 1 ml buffer (1×0.5-cm quartz cuvette, 20°C) containing a constant P14A concentration between 4 and 11 μM, so that the final lipid concentration ranged from 0.04 to 2.3 mM. A few seconds after addition of the vesicle solution the fluorescence signal was recorded and subsequently corrected for lipid and buffer contributions (contributions from the peptide could be neglected). A correction for the light scattering of vesicles, as proposed by Hellmann and Schwarz [29], was additionally taken into account. The maximal fluorescence value (reached when all peptides are membrane-bound) was determined by a procedure established by Schwarz and coworkers [29–31].

2.6. Efflux measurement

The measurements were performed at the same fluorimeter with excitation at 480 nm (slit 1.5 nm), emission at 518 nm (slit 5 nm), and a 495-nm cut-off filter. A 1×1-cm quartz cuvette contained 2 ml buffer and dye-loaded POPC vesicles at 20°C. The initial fluorescence signal F_o was measured before each run was started by adding P14A. The increasing fluorescence signal $F(t)$ was followed continuously within 20 min. To obtain the final signal F_∞ (all dye released at $t \rightarrow \infty$) a volume of 50 μl of a 10% (w/w) Triton X-100 solution was added to the cuvette. The spontaneous efflux of dye-loaded vesicles (no addition of P14A) was determined to be 0–1% after 20 min and could, therefore, be neglected in the data analysis. The lipid concentration in a cuvette ranged from 20 to 160 μM (LUV_{100}) and from 20 to 70 μM (LUV_{200}) whereas the total concentration of P14A was varied between 0.01 and 1.9 μM.

2.7. Static and transient quenching factors

The self-quenching efficiency of a dye solution entrapped in vesicles (static quenching factor Q_o) was determined as a function of the dye concentration as described previously [23,32]. The transient quenching factor (Q_t) was obtained by modifying the efflux measurements as reported elsewhere [23,32]. Briefly, P14A was added to a cuvette containing a total volume of 2.5–3 ml buffer and dye-loaded vesicles at 20°C. When the fluorescence signal $F(t)$ reached an almost stationary value (after approx. 30 min) a volume of 0.8–1 ml was transferred immediately from the cuvette to a Sephadex G50 column in order to separate the vesicles from P14A and from dye molecules being released so far. A volume of 2 ml vesicle solution was collected from the column into a new cuvette. Before and after the addition of 50 μl Triton X-100 to this vesicle solution, the fluorescence signals F_o^* and F_∞^*, respectively, were recorded. The ratio F_o^*/F_∞^* is defined as the transient quenching factor Q_t [32]. The lipid concentration ranged from 50 to 150 μM (LUV_{100}) and from 64 to 68 μM (LUV_{200}). The concentration of P14A has been varied between 0.01 and 0.4 μM.

3. Results

3.1. Secondary structure of P14A

Circular dichroism experiments gave insights into the secondary structure of P14A in various aqueous solutions. CD spectra of the melittin analogue were recorded at two different values of pH and salt content. In Fig. 1 (spectrum B) the CD spectrum of 24.5 μM P14A in buffer (107 mM NaCl, pH 7.4) is shown. According to Eq. (1) it corresponds to an α-helical content of $41 \pm 7\%$. At the same salt content but a lower pH of 5.8 a

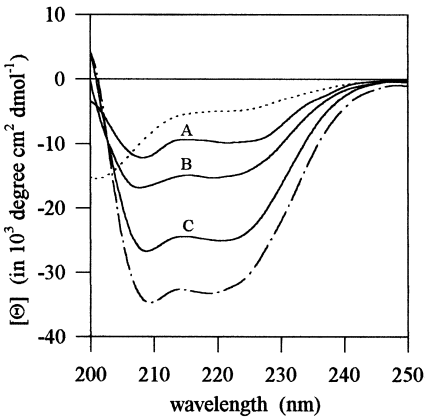

Fig. 1. Corrected and averaged CD spectra of P14A at various peptide concentrations and in different solvents: (A) 5.2 μM, (B) 24.5 μM and (C) 762 μM P14A in buffer (pH 7.4, 107 mM NaCl); dotted line, 24.5 μM P14A in water (pH 5.8); dashed–dotted line, 5.2 μM P14A bound to POPC LUV_{100} vesicles at a lipid concentration of 200 μM.

similar spectrum has been found representing an α-helical content of $46 \pm 7\%$ for a peptide concentration of 27.8 μM. Dissolving P14A at 24.5 μM in salt-free solutions like distilled water (pH 5.8) or a solution of 10 mM HEPES (pH 7.4), resulted in spectra representing a random coil structure with less than 10% helicity (Fig. 1, dotted line).

To determine the conformation of P14A in a lipid environment, 10 μM P14A was incubated with 200 μM POPC LUV_{100} vesicles in buffer. Applying the appropriate binding constant of $K_p = 5.4 \times 10^3\ M^{-1}$ (see Table 2) it was estimated that 5.2 μM peptide are bound to the membrane. After correcting the CD data for contributions from free peptide and vesicles the spectrum shown in Fig. 1 (dashed–dotted line) was obtained. It displays an α-helical content of $93 \pm 7\%$ for membrane-bound P14A. In comparison the CD spectrum of 5.2 μM P14A free in buffer has been shown (Fig. 1, spectrum A) representing an α-helical content of $27 \pm 5\%$.

3.2. Self-association of P14A

To investigate the self-aggregation tendency of P14A in comparison to the tetramerization of melittin, the CD spectra of P14A were measured in buffer (107 mM NaCl, pH 7.4) in a concentration range of 1–762 μM. The helicity at 222 nm was determined by Eq. (1). In Fig. 2a (circles) the semi-logarithmic plot of the total peptide concentration c_p vs. the α-helical content displays a sigmoidal curve. A qualitatively similar behaviour has been found for melittin [33,34]. Up to a peptide concentration of approximately 12 μM the helicity of P14A has a constant value of $28 \pm 7\%$. With further increase in peptide concentration an increase in the α-helical content occurs until a value of $75 \pm 7\%$ is reached at approximately 800 μM P14A. The spectra A–C in Fig. 1 manifest this increase in helicity. Additionally, CD spectra of P14A in water (pH 5.8, absence of salt) were recorded in a concentration range of 12–238 μM (Fig. 2a, triangles). Here, P14A remained in a random coil conformation (see Fig. 1, dotted line) and a qualitative change in the spectra was not observed within the chosen concentration range. For reasons of comparison CD spectra of melittin in water (absence of salt) were also recorded as a function of the peptide

Table 2
Parameters of membrane binding[a]

Peptide	Vesicles	K_p (in $10^3\ M^{-1}$)	z_{eff}
P14A	LUV_{100}	5.4	0
	LUV_{200}	4.0	0
Melittin[b]	LUV_{100}	5.0	1.5
	LUV_{200}	6.0	2.2

[a] Binding parameters obtained from the isotherms [Eqs. (4) and (5)] for differently sized POPC vesicles at 20°C and pH = 7.4 (see text for details). Uncertainties have been estimated as ±30% for K_p and ±10% for z_{eff}.
[b] Data from Rex and Schwarz [23].

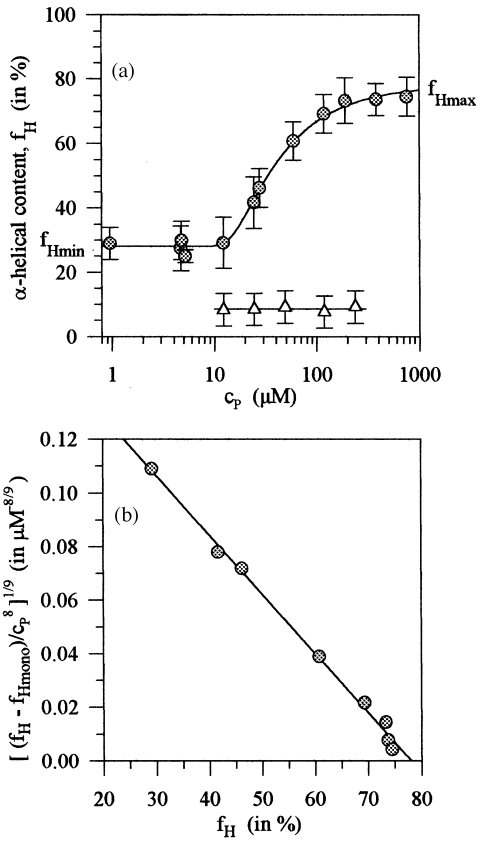

Fig. 2. Helicity of P14A as a function of peptide concentration. (a) Semi-logarithmic plot of the α-helical content f_H [calculated by Eq. (1)] of P14A in buffer (circles) and water (triangles) as a function of the total peptide concentration c_p. f_{Hmin} (= 28%) and f_{Hmax} (= 78%) indicate the helicity of P14A in monomeric and aggregated form, respectively. Eq. (2) was used to obtain the best fit for the data points. The experimental error of f_H is approximately ±7% helicity. The average value of helicity obtained for P14A in water is 8.6% and shown as a straight line. (b) Presentation of the data points of P14A in buffer (from a) according to a method described by Taylor and Kaiser [37]. The best linear regression was obtained for an aggregation number of $n = 9 \pm 1$ [Eq. (3)].

concentration in a range of 30–207 μM (data not shown). Melittin displayed a similar behaviour as P14A in water. The spectra showed mainly random coil character (see Fig. 1, dotted line).

The conformational changes which melittin undergoes with increasing peptide concentration have been explained in terms of peptide self-association [33–36]. Therefore, it seems likely to suppose that the increase in helicity of P14A is also caused by an aggregation process. To test this hypothesis gel filtration experiments were performed at various P14A concentrations using a Sephadex G50 column. Furthermore, it was investigated whether P14A at concentrations up to 12 μM exists in a monomeric or an aggregated state. As a control monomeric melittin at pH 7.4 in the absence of salt has been used [18]. Melittin eluted at approximately 9.3 ml as indicated in Fig. 3. Loading a concentration of 30 μM P14A in buffer onto the gel filtration column resulted in the elution of a large peak at approximately 9.4 ml (Fig. 3, arrow A) which is in good agreement with the control peak of monomeric melittin. The fraction collected at the peak maximum contained an approximate peptide concentration of 6 μM which falls into the concentration range ($c_p < 12$ μM) where P14A monomers would be expected (see Fig. 2a). Furthermore, a small but broad peak eluted at approximately 3.0 ml and thus indicated the existence of larger aggregates. Similar results were obtained by applying 70 μM P14A to the column. The highest injected peptide concentration was 328 μM resulting in a main peak at approximately 9.1 ml elution volume and two very broad, overlapping peaks with elution maxima at 2.9 and 5.4 ml. According to the cali-

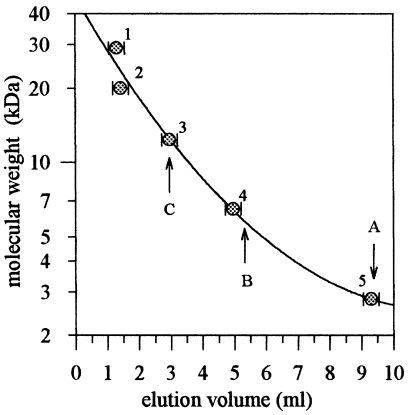

Fig. 3. Calibration of the Sephadex G50 gel filtration column by molecular weight with following proteins: (1) carbonic anhydrase (29 kDa); (2) soybean trypsin inhibitor (20 kDa); (3) cytochrome *c* (12.4 kDa); (4) aprotinin (6.5 kDa); and (5) monomeric melittin (2.8 kDa). The arrows indicate the elution volume at which significant peaks of P14A in monomeric (A) and aggregated form (B,C), respectively, were detected.

bration curve (Fig. 3) these peaks correspond to dimers and tetramers (arrows B,C) which seem to occur with a higher probability than other aggregate sizes under the chosen pH and salt conditions.

The use of gel filtration to study the concentration dependent self-association of a peptide has two drawbacks, which may limit the application of this technique. First, the injected sample will be diluted while passing through the column. Second, the method to determine the peptide content has to be sensitive enough in order to detect very low peptide concentrations per fraction. Under the gel filtration conditions chosen here, it was not possible to determine the aggregate size of P14A in the stock solution prior to sample injection. Obviously, the salt content was too low to stabilise the largest possible aggregate sizes. However, by means of the sample dilution one was able to show that P14A exists in monomeric form at low peptide concentrations. The possibility of loading the column with a low concentrated P14A solution ($c_p < 12$ μM) would have led to difficulties in the determination of peptide content per fraction. A modified Lowry assay [28] was found to be sensitive enough to detect peptide concentrations as low as 2–3 μM.

Based on the results of the gel filtration experiments, the CD data shown in Fig. 2a were analysed further. Generally, the self-association process of P14A in buffer can be described as equilibrium:

$$n\ \text{Monomer} \leftrightarrow \text{Aggregate}$$

where n is the degree of aggregation. The equilibrium constant of the aggregation process is expressed as $K_{aggr} = A_n/A^n$, where A and A_n are the equilibrium concentrations of monomers and aggregates, respectively. Combining K_{aggr} with the total peptide concentration $c_p = A + nA_n$ and the relation $A/c_p = (f_{Haggr} - f_H)/(f_{Haggr} - f_{Hmono})$ the following equation was derived:

$$c_p = (f_{Hmono} - f_{Haggr}) \cdot \left\{ (f_H - f_{Hmono}) \Big/ \left[nK_{aggr} \cdot (f_{Haggr} - f_H)^n \right] \right\}^{1/(n-1)} \quad (2)$$

where f_H is the α-helical content in percent as it was calculated from the experimental mean residue ellipticity [see Eq. (1)]. The quantities f_{Hmono} and f_{Haggr} correspond to the α-helicity of the monomeric and the highest aggregated state, respectively, and are indicated in Fig. 2a. The unknown parameters in Eq. (2) are the aggregation constant K_{aggr}, the aggregation degree n and f_{Haggr}. They can be determined by applying a method proposed by Taylor and Kaiser [37]. Accordingly, Eq. (2) is converted into the expression:

$$\left[(f_H - f_{Hmono})/c_p^{n-1} \right]^{1/n} = \left[nK_{aggr}/(f_{Haggr} - f_{Hmono})^{n-1} \right]^{1/n} \cdot (f_{Haggr} - f_H) \quad (3)$$

The total peptide concentration c_p and f_{Hmono} (= 28%) are known quantities. Thus, by plotting f_H vs. the left hand side of Eq. (3) a straight line will be obtained for an appropriate value of n. The best linear regression curve was found for $n = 9 \pm 1$ as shown in Fig. 2b. By inserting the value of n into Eq. (3) the values for f_{Haggr} and K_{aggr} can be determined [37]. Thus, a maximal value of helicity for P14A of $f_{Haggr} = 78\%$ and an aggregation constant of $K_{aggr} = 5.54 \times 10^{36}$ M^{-8} have been obtained.

To provide further evidence that the P14A aggregates are larger than melittin tetramers, the aggregate size of both peptides was estimated by dynamic light scattering. For 762 μM P14A in buffer an averaged hydrodynamic radius of 1.8 ± 0.2 nm was found. Tetrameric melittin (pH 7.4, 1 M NaCl) at peptide concentrations of 14 and 135 μM gave a hydrodynamic radius of 1.0 ± 0.1 nm which demonstrated that a P14A aggregate is approximately twice as large as a melittin tetramer. These findings are in good agreement with the CD results.

Furthermore, it was observed in NMR line width measurements that aggregates formed by P14A are larger than aggregates formed by melittin (C.E. Dempsey, personal communication).

3.3. Binding of P14A to membranes

The binding affinity of P14A to differently sized POPC liposomes (LUV_{100}, LUV_{200}) was studied by resonance energy transfer between the tryptophan residue of P14A and the NBD group of NBD-PE lipids in the membrane [29]. The peptide concentration was kept constant while the lipid concentration was gradually increased by titrating a vesicle solution. The experiment has been repeated for three to four different peptide concentrations. The binding curves obtained were analysed as described previously [31,38] in order to derive a binding isotherm for each vesicle system.

The binding of a peptide to a membrane can generally be described as a partitioning equilibrium of the peptide between aqueous phase and membrane: Peptide (free) + Lipid $\leftrightarrows$ Peptide (bound) whereby the partition coefficient K_p is defined as:

$$K_p = r \cdot \alpha / c_f \quad \text{with} \quad r = c_b / c_L \tag{4}$$

where c_L is the total lipid concentration and c_f, c_b are the equilibrium concentrations of free and bound peptide, respectively. The activity coefficient α which takes into account the electrostatic repulsion between charged, membrane-bound peptides, was expressed by the Gouy–Chapman approach as:

$$\alpha(r) = \exp[2 \cdot z_{eff} \operatorname{arcsinh}(z_{eff} \cdot b \cdot r)] \tag{5}$$

where z_{eff} is the effective charge of a bound peptide and b is a dimensionless parameter being related to the ionic strength of the aqueous phase. Under the buffer conditions applied here, a value of $b = 11.5$ was determined. In the ideal case of negligible electrostatic interactions between bound peptides ($z_{eff} = 0$, $\alpha = 1$) the binding isotherm is linear and the partition coefficient K_p is given by its slope. In the non-ideal case where electrostatic interactions interfere with the binding ($z_{eff} \neq 0$), deviations from the linear behaviour will be observed.

In Fig. 4 the isotherms for P14A binding to POPC LUV_{100} and LUV_{200} vesicles, respectively, are presented. The binding parameters K_p and z_{eff} were determined from the best fit using Eqs. (4) and (5) and are summarised for each membrane system in Table 2. For comparison the isotherm for melittin binding to POPC LUV_{200} vesicles is shown in Fig. 4 as a dotted line.

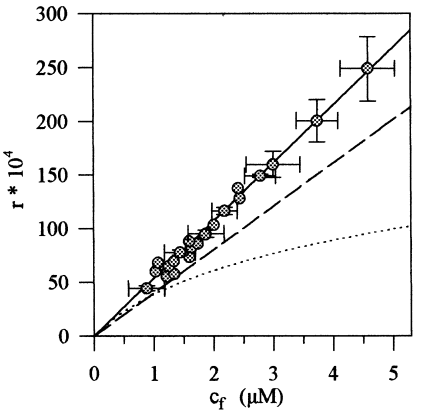

Fig. 4. Binding of P14A to POPC LUV_{100} and LUV_{200} vesicles, respectively, in buffer. For clarity only the data set for LUV_{100} is shown. The binding isotherms for LUV_{100} (continuous line) and LUV_{200} (dashed line) represent the best fit of the binding data. The values of the fitting parameters K_p and z_{eff} are given in Table 2. For comparison the isotherm of melittin binding to POPC LUV_{200} vesicles is shown (dotted line) which has been calculated from the binding parameters published by Rex and Schwarz [23].

Interestingly, the binding isotherms for P14A were found to be linear in the studied concentration range compared to the non-linear binding curve reported for melittin [23]. This fact is mainly reflected in the different z_{eff} values for P14A and melittin. Whereas bound melittin possesses an effective charge of approximately +2, the binding data for P14A could only be fitted by setting $z_{eff} = 0$ in Eq. (5). Obviously, the net charge of membrane-bound P14A is drastically reduced so that the repulsion between bound peptides becomes negligible.

The curvature of the membrane vesicles has a slight influence on the membrane binding of both peptides. The tendency to bind less to LUV_{200} vesicles than to LUV_{100} vesicles is the same for P14A and melittin [23]. Obviously, the less dense packed lipid bilayer of LUV_{100} vesicles contains more membranous defects enabling the peptide to incorporate better into the bilayer. However, at low peptide concentrations where the usual efflux

curves were obtained ($r \leq 0.001$, $c_f \leq 0.3$ μM; see below), the affinity of P14A towards LUV_{100} and LUV_{200} vesicles is very similar.

The total peptide concentration in the binding experiments ranged between 4 and 11 μM. According to the CD data (Fig. 2a) and the gel filtration experiments (Fig. 3), it can be assumed that P14A is in a monomeric state within this concentration range. At concentrations approximately 11 μM the existence of a very small number of aggregates cannot be ruled out completely, however, a contribution to the binding equilibrium seems to be negligible.

3.4. Efflux and mode of dye release

To study the leakage potential and the pore formation kinetics of P14A the fluorescent dye carboxyfluorescein was entrapped into POPC vesicles at a self-quenching concentration. The empirical efflux function $E(t)$ is obtained from the measured fluorescence signal $F(t)$ as:

$$E(t) = [F_\infty - F(t)]/(F_\infty - F_o) \quad (6)$$

where F_o and F_∞ are the fluorescence signals prior to addition of peptide and after addition of detergent, respectively. $E(t)$ describes the marker content within the vesicles, which decreases according to the normalisation from 1 towards 0 with progressing time.

For a qualitative comparison of the efflux curves, the ratio of bound peptide per lipid, $r = c_b/c_L$, was determined for each curve by means of the binding data in Table 2. In Fig. 5a three examples of efflux curves with LUV_{100} vesicles are presented (curves A–C). As expected, the induced efflux increases with increasing number of bound P14A per lipid. The dashed line in Fig. 5a is an example for the leakage from LUV_{200} vesicles which was recorded for the same value of $r = 1.84 \times 10^{-4}$ as curve B (LUV_{100}). For a similar number of bound peptides per lipid the induced leakage is enhanced for LUV_{200} vesicles which have an increased packing density of lipids and are less bent than LUV_{100} vesicles. In addition a curve of melittin-induced efflux from POPC

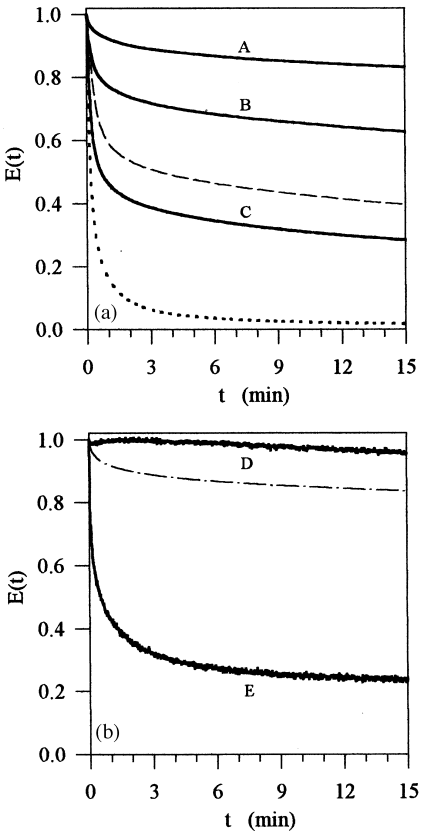

Fig. 5. Efflux curves $E(t)$ of P14A-induced leakage of differently sized marker molecules from POPC vesicles. (a) Efflux of CF from LUV_{100} at various values of bound peptide per lipid, r. (A) $r = 0.51 \times 10^{-4}$, (B) $r = 1.84 \times 10^{-4}$ and (C) $r = 3.04 \times 10^{-4}$. For comparison the efflux curves of CF from LUV_{200} induced by P14A ($r = 1.87 \times 10^{-4}$, dashed line) and by melittin ($r = 1.86 \times 10^{-4}$, dotted line) are included. (b) Efflux of FITC-dextran from LUV_{100} induced by P14A at $r = 0.72 \times 10^{-4}$ (D) and $r = 35.2 \times 10^{-4}$ (E). The dashed–dotted line represents the efflux of CF at a comparable ratio $r = 0.74 \times 10^{-4}$ under the same experimental conditions as in (D).

LUV_{200} vesicles at $r = 1.86 \times 10^{-4}$ is presented (Fig. 5a, dotted line). The efflux curve for P14A at a comparable value of r (dashed line) shows less leakage for P14A than for melittin demonstrating that under the same experimental conditions at a similar number of bound peptides per lipid, the lytic potential of P14A is reduced in comparison to melittin. The higher leakage capability of melittin over P14A was found for LUV_{100} and LUV_{200} vesicles (data not shown).

In addition to the small fluorescent marker carboxyfluorescein (0.5 nm in radius [39]) the larger marker molecule FITC-dextran (2–3 nm in radius [22]) was used. In Fig. 5b it is shown that at low values of bound peptide per lipid ($r = 0.7 \times 10^{-4}$) P14A causes the release of carboxyfluorescein (dashed–dotted line) but not of FITC-dextran (curve D) from LUV_{100} vesicles. This observation suggests that the pores formed by P14A at low concentrations have a cut-off size somewhere between the size of CF and FITC-dextran. Interestingly, at much higher r values (e.g. $r = 35.2 \times 10^{-4}$) a significant leakage of FITC-dextran can be detected (Fig. 5b, curve E) which indicates that either the diameter of the pore has drastically increased or the vesicles are disrupted by the high number of bound peptide per lipid. However, the latter case could be ruled out as shown below. The data presented here give a first indication that the size of a P14A pore seems to be a function of the number of bound peptides per vesicle and increases with increasing value of r. Qualitative similar results were found for a melittin pore. Encapsulated FITC-dextran was released from LUV_{100} vesicles by melittin at r-values larger than 4×10^{-4}, whereas for $r = 2 \times 10^{-4}$ no leakage of dextran molecules occurred (S. Rex, unpublished results).

For a more quantitative analysis of the efflux curves towards a mechanism of pore formation one has to consider the fact that the measured fluorescence signal $F(t)$ does not necessarily correspond to the total amount of leakage in a cuvette. $F(t)$ reflects the overall fluorescence intensity emitted by the released and the still encapsulated marker molecules. As described previously in detail [32,40], a correction has to be included into the data analysis in dependence on the mode of dye release. Two different modes of dye release can be distinguished. First, in an all-or-none mode all marker molecules are released from a vesicle once a pore has opened. Thus, the efflux curves describe the actual content of retained marker molecules. Second, in a graded mode the entrapped dye molecules are only partially released so that $E(t)$ has to be corrected and transformed into a retention function $R(t)$ [23,32]:

$$R(t) = [(1 - Q_o)/(1 - Q_t)]E(t) \quad (7)$$

This function represents the fraction of dye molecules which are retained inside the vesicles. In the case of an all-or-none release, where ideally $Q_t = Q_o$, the function $R(t)$ is simply described by $E(t)$.

The self-quenching efficiency of carboxyfluorescein as a function of its concentration has been determined previously [23,32]. In the case of FITC-dextran solubility problems occurred at concentrations above 10 mM so that the self-quenching efficiency of this dye as a function of its concentration could not be studied further. Due to these difficulties no information about the mode of dye release was obtained and a more quantitative analysis of the efflux curves with FITC-dextran was not possible.

To determine the mode of carboxyfluorescein release, the efflux experiments were modified as described in Section 2. To each value of the transient quenching factor Q_t a corresponding value of $E(t)$ was obtained as shown in Fig. 6 for POPC LUV_{100} vesicles. By fitting the $E(t) - Q_t$ data as explained previously in detail [32], a retention factor ρ was obtained which describes the

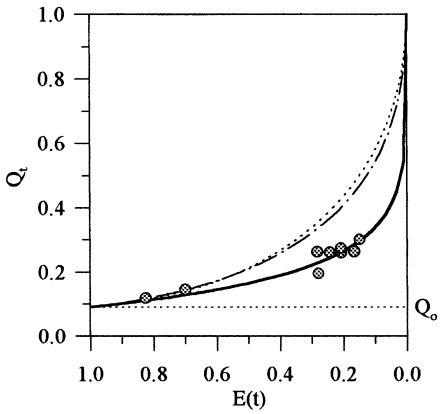

Fig. 6. Transient quenching factor Q_t as a function of the extent of efflux $E(t)$ determined for P14A and POPC LUV_{100} vesicles. The continuous line presents the best fit of the data with $Q_o = 0.0915$ and a retention factor $\rho = 0.46$. The dotted lines describe the extreme cases of an all-or-none-release ($\rho = 0$, $Q_t = Q_o$) and a graded release ($\rho \to 1$, $Q_t \gg Q_o$), respectively. For comparison the $E(t) - Q_t$ curve for melittin interacting with LUV_{100} vesicles is shown as dashed–dotted line ($\rho = 0.91$).

average fraction of dye being retained in a vesicle after one pore had been opened [40]. The retention factor ρ can be expressed in relation to the average lifetime of a pore τ_p and the relaxation time τ_o of marker efflux through a single pore [32,40]:

$$\rho = \tau_o/(\tau_o + \tau_p) \quad \text{or} \quad \tau_p/\tau_o = 1/\rho - 1 \tag{8}$$

For an all-or-none mode of dye release one would ideally find $\rho = 0$ and thus, $\tau_p/\tau_o \to \infty$ because the lifetime of a pore will be much larger than the relaxation time of the marker. In case of an extreme graded release, the retention factor ρ will approach a value of 1 and thus, $\tau_p/\tau_o \to 0$ because the lifetime of a pore is very short compared to the relaxation time so that the vesicle content leaks extremely slowly.

In Table 3 the values of both quantities, ρ and τ_p/τ_o, are given for LUV_{100} and LUV_{200} vesicles. In both vesicle systems CF is released in a graded manner whereas the lifetime of a P14A pore and the relaxation time of CF are of approximately the same magnitude since their ratio $\tau_p/\tau_o \approx 1$. The effect of the vesicle size on the mode of dye release is negligible. The ρ values for melittin [23] are approximately twice as large as for P14A, which indicates an enhanced graded efflux for the native peptide. Furthermore, the magnitude of the lifetime of a melittin pore is smaller than the relaxation time of CF by a factor of 10 (LUV_{100}) and 5 (LUV_{200}), respectively. The vesicle size seems to play a slightly more significant role for melittin than for P14A.

Table 3
Single pore retention factors[a]

Vesicles	P14A	Melittin[b]
LUV_{100}	0.46 (1.17)	0.91 (0.10)
LUV_{200}	0.44 (1.27)	0.83 (0.20)

[a] The retention factor ρ for P14A and differently sized POPC vesicles were determined as described in the text. The S.D. was estimated to be ±0.05. The ratio of the average pore lifetime to the relaxation time of marker efflux through a single pore, τ_p/τ_o, is given in parentheses as calculated from Eq. (8).

[b] Data from Rex and Schwarz [23].

The possibility that the peptide-induced efflux was caused by disrupture or fusion of the vesicles could be excluded in a series of control experiments. Hydrodynamic radii and size distributions of LUV_{100} vesicles incubated with P14A were investigated by dynamic light scattering under identical conditions as in the efflux experiments. The radius of untreated LUV_{100} has been determined as 53 ± 3 nm [22]. For r values of 4.2×10^{-4}, 21×10^{-4} and 101×10^{-4} hydrodynamic radii of 51, 50 and 52 nm, respectively, were found indicating that the vesicle size has not changed after incubation with P14A. Changes in the vesicle size distribution have also not been observed and the formation of mixed micelles could be excluded as well. For melittin, similar control experiments were carried out in a previous study [22].

All efflux measurements have been performed at total P14A concentrations much less than 2 μM. Hence, the presence of P14A aggregates in solution can be excluded (see Fig. 2a).

3.5. Pore formation kinetics

After determining the retention factor ρ the retention function $R(t)$ was converted into a function $p(t)$ in order to gain more information about the underlying pore formation kinetics. $p(t)$ describes the average number of pores per vesicle being opened within time t [40]. The following equation has been proposed empirically [23,41]:

$$p(t) = (\upsilon_1/k_1)[1 - \exp(-k_1 t)] + (\upsilon_2/k_2)[1 - \exp(-k_2 t) + \upsilon_3 t] \tag{9}$$

where k_1, k_2, υ_1, υ_2 and υ_3 are rate parameters which are obtained from the fit. The pore formation rate per vesicle is defined as $\upsilon(t) = \mathrm{d}p(t)/\mathrm{d}t$ which results in $\upsilon(t) = \upsilon_1 \times \exp(-k_1 t) + \upsilon_2 \exp(-k_2 t) + \upsilon_3$. Thus, three further rate parameters can be introduced [23]: (i) the initial pore formation rate υ_o at $t = 0$ as $\upsilon_o = \upsilon_1 + \upsilon_2 + \upsilon_3$; (ii) the intermediate pore formation rate $\upsilon_i = \upsilon_2 + \upsilon_3$; and (iii) the pore formation rate υ_∞ as $\upsilon_\infty = \upsilon_3$ when $t \to \infty$.

Table 4
Pore formation rate parameters[a]

Peptide	Vesicles	$k1$	$k2$	$v_o =$	$v_i =$	$v_\infty =$
		(in 10^{-2} s^{-1})		(in s^{-1})		
P14A	LUV_{100}	9.1	0.83	$377r + 0.27r^{0.5}$	$0.27r^{0.5}$	$0.025r^{0.5}$
	LUV_{200}	8.0	0.81	$124r + 0.23r^{0.5}$	$0.23r^{0.5}$	$0.023r^{0.5}$
Melittin[b]	LUV_{100}	5.0	0.50	$960r$	$225r$	$17r$
	LUV_{200}	5.0	0.65	$1700r$	$313r$	$20r$

[a]The rate parameters of pore formation of P14A in differently sized POPC vesicles were obtained from the analysis of efflux curves as described in the text [Eq. (9)]. S.D. were estimated to be $\pm 30\%$.

[b]Data from Rex and Schwarz [23]. For better comparison the originally given v^* data were converted into the values v as described in the text.

To perform the quantitative analysis, the efflux data $E(t)$ were converted into the corresponding function $p(t)$ and fitted by Eq. (9). The values obtained for the rate parameters have been studied as a function of the number of bound peptide per lipid, r. In a double-logarithmic plot (Fig. 7) the results of this analysis of the rate parameters v_1, v_2 and v_3 for POPC LUV_{100} vesicles are presented. The slope of the best fit of each data set reflects the underlying reaction order. For v_1, a slope of 1.0 was found indicating that the rate parameter depends linearly on r, whereas for v_2 and v_3 a slope of approximately 0.5 was determined. The rate parameters k_1 and k_2 were averaged in the form of ln k and found to be constant. Their values are given in Table 4. Additionally, v_o, v_i and v_∞ were determined as described above and the resulting functions of r are displayed in Table 4. For reasons of comparison the melittin data [23] are listed additionally. The v^* data from [23] were recalculated into v data as described therein (by multiplication with the number of lipids per vesicles) in order to have an equal basis for comparison with the data of P14A.

Except for the initial rate of pore formation v_o, the rate parameters for LUV_{100} and LUV_{200} are very similar, especially if one takes into account a S.D. of 30%. Only in the initial reaction steps of the pore formation process, the vesicle size seems to have an effect on the P14A induced leakage of CF. For melittin similar conclusions can be drawn. The rate constant k_1 is in all cases approximately 10 times larger than k_2, independent of peptide and vesicle system. Comparing both peptides, the rate constants k_1 and k_2 for P14A are by a factor of 1.5–2 larger than those for melittin. The dependencies of the rate parameters v_o, v_i and v_∞ on r differ significantly between both peptides. In general, it reveals that the pore formation mechanism for P14A is different and obviously more complex than the one proposed for melittin [23]. This statement is supported by efflux data showing that at r values above 10×10^{-4} (LUV_{100}) and above 6×10^{-4} (LUV_{200}) the complexity of the pore formation kinetics increases even further, as reported below.

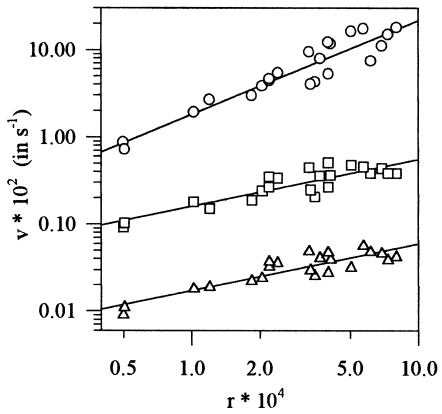

Fig. 7. Double-logarithmic plots of the rate parameters v_1 (circles), v_2 (squares) and v_3 (triangles) are shown as a function of r, determined for P14A and POPC-LUV_{100}. The straight lines correspond to the best fit of each data set with a slope of approximately 1.0 for v_1 and approximately 0.5 for v_2 and v_3 (see text for details).

3.6. Efflux behaviour at high values of r

The efflux data which have been used so far for kinetic analysis were obtained at low values of r. The distinction between low and high values of bound peptides per lipid became necessary when a qualitative and quantitative change of the P14A-induced leakage of CF from vesicles was observed with increasing r values. This change in leakage behaviour has been measured in both vesicle systems. The time course of efflux curves at high r values was found to deviate from the usually observed efflux curves at low r values of P14A. Several examples of this change in the efflux time course with increasing concentration of P14A at a constant lipid content are shown in Fig. 8. Curves A,B represent usual efflux curves and were analysed and fitted in the manner described above. However, for curves C–F a reasonable good fit using Eq. (9) was not found. This suggests that the leakage mechanism, which underlies these curves, is different from the one proposed by Eq. (9). For comparison a curve of melittin-induced efflux from POPC LUV_{100} vesicles at $r = 12.4 \times 10^{-4}$ is shown (Fig. 8, dotted line). Its time course demonstrates clearly that melittin does not display a similar efflux behaviour as P14A at these high values of r. This observation suggests that also at high r values the mechanism of pore formation is different for both peptides. Furthermore, by comparing the efflux curve for melittin with curve C for P14A at a similar r, the higher lytic activity of melittin over P14A is demonstrated repeatedly.

Analysing the efflux curves at high r values the following features could be revealed. (i) Relative high concentrations of P14A are necessary to induce the deviating efflux behaviour. The lowest r values, at which this phenomenon was observed, were 10×10^{-4} (LUV_{100}) and 6×10^{-4} (LUV_{200}), respectively. (ii) The initial slopes of the $E(t)$ curves are very similar for varying high r values. (iii) Reaching approximately 80% (LUV_{100}) or 70% (LUV_{200}) leakage, respectively, the slope of an efflux curve changes relatively abrupt in a concentration-dependent manner. In both vesicle systems it takes approximately 6 s to reach these leakage levels, independent of the value of r. (iv)

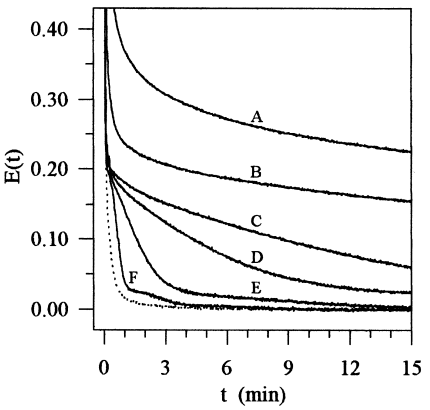

Fig. 8. With increasing ratio of bound peptide per lipid ($r \geq 10 \times 10^{-4}$ for LUV_{100}) a change in the usual time course of an efflux curve is observed. The P14A-induced leakage of CF from POPC LUV_{100} at various values of r is shown. (A) $r = 3.44 \times 10^{-4}$, (B) 5.72×10^{-4}, (C) 11.45×10^{-4}, (D) 22.8×10^{-4}, (E) 45.2×10^{-4} and (F) 88.9×10^{-4}. The lipid concentration was kept constant at 28 μM and the total P14A concentration varied from 0.073 μM (A) to 1.89 μM (F). In comparison, a time course for melittin-induced efflux in POPC LUV_{100} at $r = 12.4 \times 10^{-4}$ is presented (dotted line).

With increasing r values a second or even third change in the slope of an efflux curve can occur with time (Fig. 8, curve E,F). The higher the number of bound peptides per lipid, the shorter is the time needed to reach the conditions for an additional change in slope. In conclusion, the efflux behaviour at high r values suggests strongly that the underlying pore formation mechanism for P14A is more complex than it was derived for ordinary efflux curves at low values of r (see Table 4).

The P14A-induced leakage of FITC-dextran (Fig. 5b, curve E) at $r = 35.2 \times 10^{-4}$ does not exhibit the same unusual time course as it was observed for CF (Fig. 8, curve D,E). This observation seems to suggest that the size of a fluorescent marker has obviously an influence on the time course of a leakage experiment, most likely due to variations in the diffusion coefficient upon passing through a pore and/or due to possible dye–membrane interactions. However, the fact that FITC-dextran molecules can leak out of vesicles in a relatively high extent indicates strongly that the pores formed by P14A at high r values are larger than the pores formed at low r (see

Fig. 5b, curve D). This suggests that the size of a P14A pore is a function of r and, hence, a change in the mechanism of pore formation with increasing r can be expected.

As mentioned above, the possibility that the observed efflux at high r values was caused by disrupture or fusion of vesicles or interfered with P14A aggregates in solution, can be excluded.

4. Discussion

4.1. Effect of proline on secondary structure and self-association

Alanine is a strong helix-promoting amino acid [42] so that in general the replacement of Pro14 by an alanine residue is likely to increase the probability of α-helix formation in the case of P14A. Experimental evidence was given by ^{1}H-NMR measurements [14] and amide exchange studies of P14A in methanol [16]. It was shown that the backbone fluctuations of P14A are largely suppressed around position 14 which leads to a stabilisation of the α-helix possessing a regular, rod-like shape.

The secondary structure and the self-association process of melittin in aqueous solution have been investigated in numerous studies. In salt-free solution (ionic strength $I < 0.01$ M), melittin was found to adopt a random coil conformation which is not altered by an increase in peptide concentration [18,43,44]. Brown et al. [45] reported that melittin at 4 mM in the absence of salt (pH 7) exists in the form of monomers. The structural conformation of P14A in salt-free solution is similar to melittin and shows no variation with increasing peptide concentration (Fig. 2a). Despite the higher propensity of P14A for an α-helical conformation, such a structure seems to be prevented under salt-free conditions by a high charge density, especially at the C-terminal end. These circumstances lead also to the suppression of a self-aggregation process.

An increase in ionic strength ($I \approx 0.1$ M) at low peptide concentrations ($c_p < 10$ μM) does not affect the random coil conformation of melittin [18]. However, P14A monomers undergo a conformational change towards a higher structural content of approximately 28% helicity. A small increase in ionic strength seems to lead to a partial weakening of the electrostatic repulsive forces between the charged residues due to the presence of counterions. Approximately seven amino acids are involved in this helical structure. It is very likely that the helix-forming residues are located around position 14 according to the observed stabilisation of the amides in the central turn of the helix [14]. The presence of proline in melittin prevents any partial helical structure at low peptide and salt concentrations.

A further increase in peptide concentration under otherwise constant solvent conditions ($I \approx 0.1$ M) leads to an aggregation process for both peptides. The driving force of such a process has been ascribed to hydrophobic interactions which seem to be favoured by the proximity of peptide molecules [13], whereby the balance between electrostatic repulsion of the charged residues and the stable packing of the monomers by clustering the hydrophobic sides of the amphiphatic helices, has to be maintained. In case of melittin it has been demonstrated that the stabilisation of single helices within an aggregate is ascribable rather to the binding of counterions to the positive groups than to the formation of salt bridges [46].

The helicity of a P14A monomer in an aggregate was determined to be 78%. For tetrameric melittin similar values of helical content were found (75% [47]; 65% [48]; 75% [49]; 76% [50]). But P14A requires a considerably lower salt content in order to reach the same value of helicity as melittin. This is explained by a more efficient screening of the charged residues in case of P14A compared to melittin. Interestingly, another melittin analogue where Pro14 was substituted by a tryptophane showed also an α-helicity of approximately 75% in the aggregated state [51].

It was shown in this study that P14A aggregates are composed of 9 ± 1 monomers (Fig. 2b). The formation of aggregates larger than tetramers might have two reasons. First, P14A forms a straight α-helix, which is more rigid around position 14 than the kinked helix of melittin [16]. A rod-like shaped helix seems to have more poten-

tial to be arranged in an aggregate larger than tetramers. Second, a reduced charge density, which is caused by an improved screening of the positively charged residues, could also account for the formation of larger aggregates. Hereby, the repulsive electrostatic forces are thought to be diminished in comparison to the hydrophobic interactions between the single amphipathic helices so that the clustering of a higher number of monomers is facilitated. However, the arrangement and orientation of nine monomers within an aggregate are not known. Several possibilities for peptide arrangements within large self-associated complexes have been proposed by John and Jähnig [49].

4.2. Effect of proline on membrane interactions

Melittin is known to adopt an α-helix in membranous and micellar environments [35,43, 50,52,55]. For membrane-bound P14A an α-helical conformation has also been postulated [14] because the peptide was found to be involved in haemolysis and voltage-gated channel activities. Both peptides differ in their degree of helicity in the membrane-bound state. As shown in this study P14A adopts a structure with $93 \pm 7\%$ helicity, while melittin was reported to display a helical content of approximately 76% [50]. Again, formation of a more stable helix and an improved screening of charged residues are very likely to be the reasons for the different results. In addition, the polar headgroups of membrane lipids may contribute to the more efficient screening in case of P14A. Dempsey and Butler [55] and Okada et al. [52] demonstrated by nuclear magnetic resonance spectroscopy that the C-terminal end of membrane-bound melittin remains unstructured. Would the five C-terminal residues be involved in an α-helical conformation the charged side chains of Lys23 and Arg24 of melittin would be buried in the hydrophobic part of the lipid bilayer which is an energetically unfavourable situation [52]. For similar reasons it is very likely that the C-terminal residues of P14A do not contribute to the α-helical structure of the peptide — despite the screening of their positively charged side chains (see below). In this regard the measured value of $93 \pm 7\%$ appears to be somewhat larger than the expected value of approximately 85% (assuming 22 of the 26 residues are involved in the helix formation). This discrepancy can be mainly ascribed to experimental uncertainties, especially to the fact that the spectra have to be corrected for contributions from vesicles and free peptide (see Section 3).

The helical content of P14A in a membranous environment is higher than in its peptide aggregates ($78 \pm 7\%$). This can be explained by the amphipathic nature of the helical peptide whereby the hydrophobic half seems to be better accommodated within a lipid bilayer than within an aggregate of several identical peptides. Presumably, the shielding of the hydrophobic side chains in an aggregate is not as effective as in the membrane.

Additional evidence for the efficient shielding of the positive residues of membrane-bound P14A was given by the binding measurements with POPC vesicles. The binding isotherm of melittin deviates from a linear slope, thus indicating the presence of repulsive interactions between bound peptides which possess an effective charge of $z_{\mathrm{eff}} = +2$. In contrast, the binding isotherm of P14A was found to be linear. The effective charge of $z_{\mathrm{eff}} = 0$ shows that repulsive forces between membrane-bound peptide molecules can be neglected (Fig. 4). This indicates, furthermore, that the charged residues of the peptide, which are very likely to be exposed on the membrane–water interface, are shielded completely by counterions. At concentrations where electrostatic repulsive forces are negligible the binding of P14A and melittin towards POPC membranes is very similar, hence showing that the different structural properties do not influence the binding per se (Table 2).

4.3. Effect of proline on pore formation

Due to the differences between P14A and melittin in their structural and overall electrostatic properties it is almost expected to find deviations in efflux behaviour and pore formation kinetics for both peptides. The observation that

the P14A-induced leakage is suppressed compared to the leakage induced by melittin, might be explained by differences in their pore sizes and/or pore lifetimes. The pore lifetime τ_p and the relaxation time of the fluorescent marker τ_o are not known individually. However, the relaxation time is related to the pore size as $\tau_o \sim 1/\text{pore size}$ and from the analysis of the efflux data it is known that $\rho_{mel} \approx 2\rho_{P14A}$ (Table 3). Furthermore, it was observed that at similar values of r the actual leakage induced by melittin is larger than the one induced by P14A (Fig. 5a). Analysing these facts it can be ruled out that: (i) both peptides have identical pore sizes but differ in their pore lifetimes; and (ii) both peptides have identical pore lifetimes but differ in their pore sizes. Obviously, pore lifetime and pore size are both different for P14A and melittin. Consistent with the results mentioned above, the following two possibilities exist: (1) the pores formed by P14A are larger than melittin pores but their lifetime is much shorter; or (2) the P14A pores are much smaller but have a longer lifetime than melittin pores, in such a way that in both cases a reduced efflux for P14A will be found. The higher tendency of P14A to form aggregates in solution and the reduced net charge ($z_{eff} = 0$) of the peptide in a membrane-bound state, seems to make the first possibility very likely. The formation of P14A aggregates within the membrane surface prior to pore formation should also be taken into consideration. The analysis of the efflux curves showed a more complex nature of the mechanism of pore formation for P14A. Thus, the absence of proline influences directly (by the formation of a rod-like shaped α-helix) and indirectly (by an improved screening of charged residues leading to a zero net charge) the lytic activity of P14A.

With increasing r values P14A and melittin [53,54] change their pore size towards larger assemblies as it was demonstrated by the efflux of larger marker molecules at higher values of membrane-bound peptide per lipid. This suggests strongly that the mechanism of pore formation also underlies changes with increasing r values. Both peptides are similar in these features; however, the detailed kinetic mechanism which underlies the peptide-induced leakage is different for both peptides (Table 4).

An explanation for the unusual leakage which is induced by P14A at high r values, is not yet available. More detailed experiments would be necessary to elucidate the molecular basis of the observed macroscopic effects. However, it is very probable that at such high r values very large pores have been formed since a strong efflux of FITC-dextran was found.

Dempsey et al. [14] reported that in voltage-dependent conductance measurements the activity of P14A is suppressed compared to melittin which was ascribed to the structural differences between both peptides. Additionally, it is suggested that the difference between the peptides in their net charge may also contribute to the reduced activity of P14A.

5. Conclusions

The proline residue at position 14 and the number and distribution of positively charged residues are well conserved among the various melittin peptides of other species of honeybees (see Table 1). In this report it was confirmed that the proline residue in melittin is mainly of structural importance. Additionally, it has been observed that in the absence of proline a better exposure of the charged residues to counterions was possible which led to an improved screening of those amino acids. Thus, proline influences the overall electrostatic properties of melittin by preventing a facilitated shielding of its charged residues. Consequently, these circumstances lead to the formation of aggregates of a defined small size, to a reduced membrane binding, and to an increase in the efficiency of its lytic activity in model membranes. The functional properties of P14A and melittin show only differences in their efficiencies but are not dramatically inhibited by the Pro → Ala substitution. Therefore, it is speculated that the proline residue is the optimal amino acid at position 14 for melittin's functional features and biological activity.

6. Nomenclature

P14A: melittin analogue with Pro14 → Ala substitution
LUV_{100} and LUV_{200}: large unilamellar vesicles of 100 or 200 nm diameter, respectively
POPC: 1-palmitoyl-2-oleoyl-*sn*-glycero-3-phosphatidylcholine
DOPE: 1,2-di-oleoyl-*sn*-glycero-3-phosphatidylethanolamine
NBD: nitrobenz-2-oxa-1,3-diazol
CF: 5(6)-carboxyfluorescein
FITC: fluoresceinisothiocyanate
HEPES: *N*-(2-hydroxy-ethyl)piperazine-*N′*-2-ethanesulfonic acid
TES: *N*-tris-[hydroxymethyl]methyl-2-aminoethanesulfonic acid
EDTA: ethylenediaminetetraacetic acid
CD: circular dichroism

Acknowledgements

I am grateful to Prof. Gerhard Schwarz for his support of this project. My thanks go to Dr Chris Dempsey (Biochemistry Department and Centre of Molecular Recognition, Bristol University, UK) for his generous gift of P14A and the stimulating discussions. I would like to thank Dr Frank Stieber (Institute of Physical Chemistry of this University) for enabling the dynamic light scattering measurements, Christoph Stürzinger for technical assistance and Enrico Schleiff for help in the CD experiments and critically reading the manuscript. This study was supported by the grant No. 31-32188.91 from the Swiss National Science Foundation.

References

[1] K.T. O'Neil, W.F. Degrado, A thermodynamic scale for the helix-forming tendencies of the commonly occurring amino acids, Science 250 (1990) 646–651.
[2] J.S. Richardson, D.C. Richardson, Prediction of protein structure and the principles of protein conformation, in: G.D. Fasman (Ed.), Principles and Patterns of Protein Conformation, Plenum Press, New York, 1989, pp. 1–98.
[3] K.A. Williams, C.M. Deber, Proline residues in transmembrane helices: structural or dynamical role? Biochemistry 30 (1991) 8919–8923.
[4] D.J. Barlow, J.M. Thornton, Helix geometry in proteins, J. Mol. Biol. 201 (1988) 601–619.
[5] S.-C. Li, N.K. Goto, K.A. Williams, C.M. Deber, α-helical, but not β-sheet, propensity of proline is determined by peptide environment, Proc. Natl. Acad. Sci. USA 93 (1996) 6676–6681.
[6] M. Wellner, I. Monden, M.M. Mueckler, K. Keller, Functional consequences of proline mutations in the putative transmembrane segments 6 and 10 of the glucose transporter GLUT1, Eur. J. Biochem. 227 (1995) 454–458.
[7] C.J. Brandl, C.M. Deber, Hypothesis about the function of membrane-buried proline residues in transport proteins, Proc. Natl. Acad. Sci. USA 83 (1986) 917–921.
[8] I. Cornut, E. Thiaudière, J. Dufourcq, The amphiphatic helix, in: R.M. Epand (Ed.), The Amphipathic Helix in Cytotoxic Peptides, CRC Press, Boca Raton, 1993, pp. 173–220.
[9] A.W. Bernheimer, B. Rudy, Interactions between membranes and cytolytic peptides, Biochim. Biophys. Acta 864 (1986) 123–141.
[10] C.E. Dempsey, The actions of melittin on membranes, Biochim. Biophys. Acta 1031 (1990) 143–161.
[11] J.E. Fletcher, M.S. Jiang, Possible mechanism of action of cobra snake venom cardiotoxins and bee venom melittin, Toxicon 31 (1993) 669–695.
[12] B. Bechinger, Structure and functions of channel-forming peptides: magainins, cecropins, melittin and alamethicin, J. Membr. Biol. 156 (1997) 197–211.
[13] T.C. Terwilliger, D. Eisenberg, The structure of melittin, J. Biol. Chem. 257 (1982) 6016–6022.
[14] C.E. Dempsey, R. Bazzo, T.S. Harvey, I. Syperek, G. Boheim, I.D. Campbell, Contribution of proline-14 to the structure and actions of melittin, FEBS Lett. 281 (1991) 240–244.
[15] C.E. Dempsey, B. Sternberg, Reversible disc-micellization of dimyristoylphosphatidylcholine bilayers induced by melittin and [Ala-14]melittin, Biochim. Biophys. Acta 1061 (1991) 175–184.
[16] C.E. Dempsey, Quantitation of the effects of an internal proline residue on individual hydrogen bond stabilities in an α-helix: pH-dependent amide exchange in melittin and [Ala-14]melittin, Biochemistry 31 (1992) 4705–4712.
[17] S.V. Rudenko, E.E. Nipot, Protection by chlorpromazine, albumin and bivalent cations against haemolysis induced by melittin, [Ala-14]melittin and whole bee venom, Biochem. J. 317 (1996) 747–754.
[18] S.C. Quay, C.C. Condie, Conformational studies of aqueous melittin: thermodynamic parameters of the monomer–tetramer self-association reaction, Biochemistry 22 (1983) 695–700.
[19] J. Barbet, P. Machy, A. Truneh, L.D. Leserman, Weak acid-induced release of liposome-encapsulated carboxyfluorescein, Biochim. Biophys. Acta 772 (1984) 347–356.

[20] I. Lang, M. Scholz, R. Peters, Molecular mobility and nucleocytoplasmic flux in heptoma cells, J. Cell Biol. 102 (1986) 1183–1190.

[21] E. Poitevin, P. Wahl, Study of the translational diffusion of macromolecules in beads of gel chromatography by the FRAP method, Biophys. Chem. 31 (1988) 247–258.

[22] S. Rex, Pore formation induced by the peptide melittin in different lipid vesicle membranes, Biophys. Chem. 58 (1996) 75–85.

[23] S. Rex, G. Schwarz, Quantitative studies on the melittin induced leakage mechanism of lipid vesicles, Biochemistry 37 (1998) 2336–2345.

[24] M.J. Hope, M.B. Bally, L.D. Mayer, A.S. Janoff, P.R. Cullis, Generation of multilamellar and unilamellar phospholipid vesicles, Chem. Phys. Lipids 40 (1986) 89–107.

[25] L.D. Mayer, M.J. Hope, P.R. Cullis, Vesicles of variable sizes produced by a rapid extrusion procedure, Biochim. Biophys. Acta 858 (1986) 161–168.

[26] C.F.J. Böttcher, C.M. vanGent, C. Pries, A rapid and sensitive sub-micro phosphorus determination, Anal. Chim. Acta 24 (1961) 203–204.

[27] Y.-H. Chen, J.T. Yang, H.M. Martinez, Determination of the secondary structures of proteins by circular dichroism and optical rotatory dispersion, Biochemistry 11 (1972) 4120–4131.

[28] M.A.K. Markwell, S.M. Haas, N.E. Tolbert, L.L. Bieber, Protein determination in membrane and lipoprotein samples: manual and automated procedures, Methods Enzymol. 72 (1981) 296–303.

[29] N. Hellmann, G. Schwarz, Peptide–liposome association. A critical examination with mastoparan-X, Biochim. Biophys. Acta 1369 (1998) 267–277.

[30] G. Schwarz, H. Gerke, V. Rizzo, S. Stankowski, Incorporation kinetics in a membrane studied with the pore-forming peptide alamethicin, Biophys. J. 52 (1987) 685–692.

[31] G. Schwarz, Electrical interactions of membrane active peptides at lipid/water interfaces, Biophys. Chem. 58 (1996) 67–73.

[32] G. Schwarz, A. Arbuzova, Pore kinetics reflected in the dequenching of a lipid vesicle entrapped fluorescent dye, Biochim. Biophys. Acta 1239 (1995) 51–57.

[33] K. Ramalingam, S. Aimoto, J. Bello, Conformational studies of anionic melittin analogues: effect of peptide concentration, pH, ionic strength, and temperature-models for protein folding and halophilic proteins, Biopolymers 32 (1992) 981–992.

[34] E. Pérez-Payá, R.A. Houghten, S.E. Blondelle, The role of amphipathicity in the folding self-association and biological activity of multiple subunit small proteins, J. Biol. Chem. 20 (1995) 1048–1056.

[35] J. Bello, H.R. Bello, E. Granados, Conformation and aggregation of melittin: dependence on pH and concentration, Biochemistry 21 (1982) 461–465.

[36] Y. Goto, Y. Hagihara, Mechanism of the conformational transition of melittin, Biochemistry 31 (1992) 732–738.

[37] F.W. Taylor, E.T. Kaiser, Structure-function analysis of proteins through the design synthesis and study of peptide models, Methods Enzymol. 154 (1987) 473–498.

[38] G. Schwarz, G. Beschiaschvili, Thermodynamic and kinetic studies on the association of melittin with a phospholipid bilayer, Biochim. Biophys. Acta 979 (1989) 82–90.

[39] J. Zimmerberg, R. Blumenthal, D.P. Sarkar, M. Curran, S.J. Morris, Restricted movement of lipid and aqueous dyes through pores formed by influenza hemagglutinin during cell fusion, J. Cell Biol. 127 (1994) 1885–1894.

[40] G. Schwarz, C. Robert, Kinetics of pore-mediated release of marker molecules from liposomes or cells, Biophys. Chem. 42 (1992) 291–296.

[41] A. Arbuzova, G. Schwarz, Pore kinetics of mastoparan peptides in large unilamellar lipid vesicles, Prog. Colloid Polym. Sci. 100 (1996) 345–350.

[42] P.Y. Chou, G.D. Fasman, Prediction of the secondary structure of proteins from their amino acid sequence, Adv. Enzymol. 47 (1978) 45–148.

[43] A.F. Drake, R.C. Hider, The structure of melittin in lipid bilayer membranes, Biochim. Biophys. Acta 555 (1979) 371–373.

[44] J.F. Faucon, J. Dufourcq, C. Lussan, The self-association of melittin and its binding to lipids, FEBS Lett. 102 (1979) 187–190.

[45] L.R. Brown, J. Lauterwein, K. Wüthrich, High resolution ^{1}H-NMR studies of self-aggregation of melittin in aqueous solution, Biochim. Biophys. Acta 622 (1980) 231–244.

[46] Y. Hagihara, M. Kataoka, S. Aimoto, Y. Goto, Charge repulsion in the conformational stability of melittin, Biochemistry 31 (1992) 11908–11914.

[47] A.J. Weaver, M.D. Kemple, F.G. Prendergast, Characterization of selectively ^{13}C-labeled synthetic melittin and melittin analogues in isotropic solvents by circular dichroism fluorescence and NMR spectroscopy, Biochemistry 28 (1989) 8614–8623.

[48] J.C. Talbot, J. Dufourcq, J. deBony, J.F. Faucon, C. Lussan, Conformational change and self association of monomeric melittin, FEBS Lett. 102 (1979) 191–193.

[49] E. John, F. Jähnig, A synthetic analogue of melittin aggregates in large oligomers, Biophys. J. 63 (1992) 1536–1543.

[50] H. Vogel, F. Jähnig, The structure of melittin in membranes, Biophys. J. 50 (1986) 573–582.

[51] E. Pérez-Payá, R.A. Houghten, S.E. Blondelle, Determination of the secondary structure of selected melittin analogues with different haemolytic activities, Biochem. J. 299 (1994) 587–591.

[52] A. Okada, K. Wakamatsu, T. Miyazawa, T. Higashijima, Vesicle-bound conformation of melittin: transferred nu-

clear overhauser enhancement analysis in the presence of perdeuterated phosphatidylcholine vesicles, Biochemistry 33 (1994) 9438–9446.
[53] A.S. Ladokhin, M.E. Selsted, S.H. White, Sizing membrane pores in lipid vesicles by leakage of co-encapsulated markers: pore formation by melittin, Biophys. J. 72 (1997) 1762–1766.
[54] K. Matsuzaki, S. Yoneyama, K. Miyajima, Pore formation and translocation of melittin, Biophys. J. 73 (1997) 831–838.
[55] C.E. Dempsey, G.S. Butler, Helical structure and orientation of melittin in dispersed phospholipid membranes from amide exchange analysis in situ, Biochemistry 31 (1992) 11973–11977.